



Published in final edited form as:

Neuroimage. 2007 August 1; 37(1): 230–242.

Live Imaging of Neuronal Connections by Magnetic Resonance: Robust Transport in the Hippocampal-Septal Memory Circuit in a Mouse Model of Down Syndrome

Elaine L. Bearer^{1,2}, Xiaowei Zhang², and Russell E. Jacobs²

¹ Department of Pathology and Laboratory Medicine, Brown University, Providence, RI 02912

² Biological Imaging Center, Beckman Institute, California Institute of Technology, Pasadena, CA 91125

Abstract

Connections from hippocampus to septal nuclei have been implicated in memory loss and the cognitive impairment in Down syndrome (DS). We trace these connections in living mice by Mn^{2+} enhanced 3D MRI and compare normal with a trisomic mouse model of DS, Ts65Dn. After injection of 4 nl of 200 mM Mn^{2+} into the right hippocampus, Mn^{2+} enhanced circuitry was imaged at 0.5, 6, and 24 hr in each of 13 different mice by high resolution MRI to detect dynamic changes in signal over time. The pattern of Mn^{2+} enhanced signal in vivo correlated with the histologic pattern in fixed brains of co-injected 3kD rhodamine-dextranamine, a classic tracer. Statistical parametric mapping comparing intensity changes between different time points revealed that the dynamics of Mn^{2+} transport in this pathway were surprisingly more robust in DS mice than in littermate controls, with statistically significant intensity changes in DS appearing at earlier time points along expected pathways. This supports reciprocal alterations of transport in the hippocampal-forebrain circuit as being implicated in DS and argues against a general failure of transport. This is the first examination of in vivo transport dynamics in this pathway and the first report of elevated transport in DS.

Keywords

axonal transport; Down syndrome; MRI; tract tracing; hippocampal-forebrain connection; cholinergic neurons

Introduction

Down syndrome, trisomy 21, is the most frequent genetic cause of mental retardation (Epstein, 1986, Korenberg et al., 1994). A mouse model of Down syndrome (DS), the partial trisomic Ts65Dn, has been extensively characterized with respect to deficits in behavioral measures for learning and memory, histopathology of the brain, and functional parameters (Davisson et al., 1990, Davisson et al., 1993, Reeves et al., 1995, Olson et al., 2004, Roper and Reeves, 2006, Seregaza et al., 2006). As in human DS, Ts65Dn mice display decreased cholinergic neuron density in the medial septal nucleus (MSN) of the forebrain (Holtzman et al., 1996, Cooper et al., 2001, Salehi et al., 2003, Delcroix et al., 2004), as well as over-expression

Corresponding Author: Russell E. Jacobs M/C 139-74 Beckman Institute California Institute of Technology Pasadena, CA 91125
Telephone: 626-395-2849 Fax: 626-449-5163 Email: rjacobs@caltech.edu

Publisher's Disclaimer: This is a PDF file of an unedited manuscript that has been accepted for publication. As a service to our customers we are providing this early version of the manuscript. The manuscript will undergo copyediting, typesetting, and review of the resulting proof before it is published in its final citable form. Please note that during the production process errors may be discovered which could affect the content, and all legal disclaimers that apply to the journal pertain.

of genes encoded on the excess chromosomal segment (Holtzman et al., 1996, Hunter et al., 2003, Seo and Isaacson, 2005).

Reciprocal connections link neurons in the forebrain with those in the hippocampus. Neurons with cell bodies in the forebrain, including glutamergic, GABAergic and cholinergic neurons, send processes to the hippocampus (Amaral and Kurz, 1985, Gaykema et al., 1991, Alonso et al., 1996, Risold and Swanson, 1996, Risold and Swanson, 1997, Colom, 2006) and hippocampal pyramidal neurons innervate the septum (Wu et al., 2000). Transport within these processes is thought to be important for neuronal functioning and survival (Stokin et al., 2005). When radiolabeled nerve growth factor (NGF) is injected into the hippocampal region, less arrives in the forebrain in Ts65Dn mice compared to wildtype littermates (Cooper et al., 2001). This has been attributed to decreased retrograde transport in TrkA expressing cholinergic neurons and thus is proposed to underlie the cholinergic neuronal atrophy in these mice. Treatment with NGF by intracerebroventricular injection in Ts65Dn mice, nonhuman primates, and Alzheimer's patients results in recovery of basal forebrain cholinergic cells expressing the NGF receptor, TrkA (Tuszynski et al., 1990, Cooper et al., 2001, Tuszynski et al., 2005). Thus, decreased transport of NGF from hippocampus to forebrain may play a significant role in DS, although direct imaging of such transport is lacking. Recent work also implicates transport in this pathway as a causative factor in Alzheimer's disease, where axonal varicosities presumed to represent transport blockages were found in cholinergic neurons projecting from septum to hippocampus (Stokin et al., 2005). Taken together these results suggest that generalized defects in transport may result in cognitive dysfunction and neuronal degeneration.

Here we test whether connections from the hippocampus to the forebrain are altered in DS mice. We use Mn^{2+} enhanced magnetic resonance imaging (MEMRI) to image this circuit in living DS mice and their normal 2N littermates. Mn^{2+} is a T_1 MR contrast agent that enters neurons through calcium channels (Merritt et al., 1989), is carried down the axon primarily by anterograde transport (probably via transport vesicles), and crosses synapses (Lin and Koretsky, 1997, Pautler et al., 2003, Silva et al., 2004). In the macaque, stereotaxic co-injection of Mn^{2+} and the classic histologic tracer, wheat germ agglutinin conjugated to horse radish peroxidase, yielded the same highly specific projection pattern (Saleem et al., 2002, Murayama et al., 2006), further demonstrating the usefulness of Mn^{2+} as a trans-synaptic tracer of neuronal connections.

We injected nanoliter volumes of Mn^{2+} into a precise location in the right hippocampus of 7 Ts65Dn and 6 2N littermates and imaged the living mice by MR at 0.5, 6 and 24 hr afterwards. To obtain statistically reliable information, we performed 3-dimensional statistical analyses of Mn^{2+} -induced changes of intensity over time. First images obtained at the same time point from all mice in either the Ts65Dn or 2N littermates group were warped into one 3D space (Lancaster et al., 2003, Kovacevic et al., 2005, Lee et al., 2005). By taking the average intensity of each voxel from all warped images in each group a single averaged 3D image for each genotype at each time point was generated. Datasets from two different time points were compared using the paired Student's *t*-test to identify those voxels whose intensity changed significantly between time points. Co-injection of the classical histological tracer, 3kD rhodamine-dextran-amine (RDA), followed by post-mortem microscopic analysis confirmed our MR methodology. In contrast to studies showing decreased NGF transport in DS mice, we find robust transport in these mice of these general tract tracers. Similarities in the molecular machinery used in anterograde and retrograde transport allows us to draw conclusions about general transport dysfunction in the DS mouse.

Material and Methods

Animals

Nine to eleven month old Ts65Dn mice and 2N littermates were obtained from Jackson Labs (Bar Harbor, ME). Seven Ts65Dn (trisomic) and six 2N littermates (wildtype) mice were employed in this study. All mice were male. Genotypes were confirmed by Cecilia Schmidt (Jackson Labs) by quantitative PCR (Liu et al., 2003). All animal experiments conformed to National Institutes of Health guidelines and were approved by the California Institute of Technology Animal Care and Use Committee.

Stereotaxic Injection

Calibrated micropipettes were used to attain consistent injection volumes. The micropipettes were fashioned from 1 mm OD quartz capillary pulled to approximately 40 μ m ID bore near the tip with a Sutter Instruments (Novato, CA) P-2000 micropipette puller. The identical program was used to pull all micropipettes. Micropipettes were calibrated by drawing a 4mm length of the MnCl₂/RDA solution (see below) into the end of the micropipette using a World Precision Instruments Inc. (Sarasota, Florida) microsyringe pump with digital display driving a 10 μ l syringe fitted to the micropipette via oil-filled 0.01" ID PEEKTM (polyetheretherketone) tubing (Upchurch Scientific Inc, Oak Harbor, WA). The total solution volume was slowly ejected into a small amount of oil on a hemocytometer using the microsyringe pump, and the volume of the spherical drop determined from measurement of its diameter. Performing this procedure with six different micropipettes yielded a volume of 4.3 \pm 0.6 nl (average \pm standard deviation) for the delivered material. The same apparatus and filling/ejection procedure was used for stereotaxic injections.

Ts65Dn and 2N littermate mice were anesthetized with ketamine/xylazine (7.5mg ketamine plus 5mg xylazine per kg, i.p) and placed in a stereotaxic frame (Kopf Instruments, Tujunga, CA). 4.3 nl of 200 mM MnCl₂ with 0.5 mg/ml RDA (3k) (Molecular Probes/Invitrogen, Eugene, OR) was injected unilaterally into the right hippocampus (coordinates x -3.2 mm (midline), y -4.1 mm (Bregma), z 3.4 mm (down) (Paxinos and Franklin, 2001)) over 5 minutes using the microsyringe pump and calibrated micropipette in a modified procedure (Bearer et al., 2000, Jaffe and Terasaki, 2004). After injection, the capillary was left in place for 3-5 minutes and withdrawn over 5 minutes. Animals were injected and imaged over a 3 week time period in random order.

Following injection, the animal was immediately placed in the MR scanner under 0.8% isoflurane anesthetic. Inspection of MR images recorded 0.5 hr after injection revealed that the average injection site (center of the small hypointense region) for the Ts65Dn mice was: x (lateral) +3.43 \pm 0.37 mm; y (A-P), -3.55 \pm 0.4 mm, z (D-V) -4.07 \pm 1.5 mm; and for 2N littermates was: x , +3.27 \pm 0.22 mm; y , -4.23 \pm 0.23 mm; z , -3.05 \pm 0.26 mm.

Magnetic Resonance Imaging

An 11.7T 89 mm vertical bore Bruker BioSpin Avance DRX500 scanner (Bruker BioSpin Inc, Billerica, MA) equipped with a Micro2.5 gradient system was used to acquire *in vivo* mouse brain images with a 35 mm linear birdcage RF coil. The animal's head was secured in a Teflon stereotaxic unit within the RF coil to minimize movement and aid in reproducible placement. Temperature and respiration were continuously monitored during data acquisition and remained within normal ranges. We employed a 3D RARE imaging sequence (Hennig et al., 1986) with RARE factor of 4, 4 averages, TR/TE_{eff} = 300ms/21ms; matrix size of 256 \times 160 \times 128; FOV 23 mm \times 14.4 mm \times 11.5 mm; yielding 90 μ m isotropic voxels with 102 minutes scan time. Images were recorded from each mouse before (1-5 days) and after injection

(0.5 hr, 6 hr, and 24 hr). All 13 mice (7 Ts65Dn and 6 2N littermates) were imaged at each of these 4 time points.

Histology

One day to 3 weeks after *in vivo* MR imaging, each mouse was anesthetized, sacrificed and fixed by transcardial perfusion with a 30 ml washout with warm heparinized phosphate buffered saline (PBS) followed by 30 ml of room temperature 4% paraformaldehyde (PFA) in PBS at a rate of 5 ml/min. The carcass was decapitated and the head rocked in 4% PFA in PBS overnight at 4°C. Brains dissected from the calvarium were sent to Neuroscience Associates (NSA, Knoxville, TN) for gelatin embedding, frozen sectioning at 35 µm and staining. Alternate sections were selected for staining with either Thionine/Nissl for cellular morphology, or immunohistochemistry for anti-choline acetyl transferase (ChAT), a relatively specific marker for cholinergic neurons, or for mounting unstained in anti-quench (Vector Lab, Burlingame, CA) to image the RDA fluorescence. Sections were imaged on a Zeiss Axioscope equipped with 5×, 10×, 20×, 40×, 63× and 100× neofluor objectives and captured by an Axioicam MRM. The number of ChAT positive neurons in the MSN was obtained from three trisomic and three 2N littermates embedded in the same gelatin block and sectioned in parallel simultaneously in register. Four sections traversing the MSN were selected for counts, and all six brains were counted in each section. The anterior commissure was used as a landmark to confirm equivalency of the position of the section for each brain along the A-P axis. More than 1,000 cells were counted for each animal.

Image Processing and Derivation of Statistical Parametric Maps

MR image data was converted to Analyze 7.5 format (Mayo Clinic, Rochester, MN) modified to be readable in SPM2 (Wellcome Department of Imaging Neuroscience, University College London). SPM2 was used for all statistical comparisons in a manner similar to Cross and coworkers (Cross et al., 2004). After bias correction in SPM2, each was scaled to the mode of its intensity histogram (Kovacevic et al., 2005). Initially, one of the wildtype pre-injection images was chosen as a template and all 52 images (all animals at all time points) were normalized to it using an affine transformation and interpolated to 50µm voxel size. The average of the normalized pre-injected images from the wildtype group and from the DS group were each calculated and used as template images for their respective groups; removing bias due to selection of any individual image as template (Kovacevic et al., 2005, Lee et al., 2005). Pre-injected DS and 2N brain images were then normalized to their respective averages using full nonlinear normalization. The nonlinear transformation used to drive each individual mouse's pre-injected scan into its template was re-applied to drive that mouse's 0.5, 6, and 24 hr scans into the same coordinate system. Images were smoothed to 300µm and paired Student's *t*-tests performed comparing the different time points within each group, providing *t*-value and corresponding p-value maps of significant differences. The averaged images shown in Figures 3, 5 and 6 represent the arithmetic mean of each voxel in the smoothed DS or 3N littermate individual images.

Computational Rendering:

Visualization of the MR images and statistical parametric maps was performed with ResolveRT4 (Mercury Computer Systems, Inc., Hudson, NH) and MRicro (Rorden and Brett, 2000).

Volumetric analysis of enhanced voxels:

For each of the 13 half hour data sets, the number of voxels within injection site halo were determined using the 3D ROI feature in MRicro. The halo was defined as contiguous voxels

around the injection site with intensity greater than the mean unenhanced parenchyma intensity plus 3 times the background noise level.

The 3D maps of voxels with significantly increased intensity between each pair of images (0.5 hr versus preinjection, 6 versus 0.5 hr, and 24 versus 6 hr) were used to determine the volume of brain displaying Mn^{2+} enhanced signal in each group. The number of voxels within a defined anatomical region whose intensity was enhanced ($p < 0.0005$) was computed using MRIcro.

Results

The Ts65Dn genotype was confirmed by PCR and the phenotype by histologic examination of individual mice fixed by perfusion after MRI (Fig. 1). Ts65Dn mice displayed the expected morphological phenotype of decreased cell numbers and loss of cholinergic neurons in the septal nuclei (Fig. 1), as previously reported (Granholm et al., 2000, Cooper et al., 2001, Seo and Isacson, 2005). Histological examination revealed qualitative decreases in the number and size of cells in the septal nuclei of DS mice as compared to 2N littermates (Fig. 1A and B). Immunohistochemistry with anti-choline acetyl transferase (ChAT) demonstrated diminished numbers of cholinergic neurons in the medial septal nuclei (MSN) of DS mice versus 2N littermates (Fig. 1C). In six of the mice, counts of ChAT positive nuclei in histologic sections spanning the MSN demonstrated a $30 \pm 5\%$ decrease in the number of neurons in DS versus 2N littermates. ChAT-positive neuronal cell bodies found in the MSN of DS brains also appeared shrunken compared to the plump cell bodies in littermates. No obvious differences in thickness or number of fibers in the hippocampal commissure, fimbria, or fornix were observed in histological sections. Thus, the aging Ts65Dn mice used in this study displayed the expected morphological abnormalities previously described for these mice, features similar to those found in human Alzheimer's disease and Down syndrome.

Injection site analysis by correlation of optical and MR microscopy

Co-injection of the tracer, RDA, with the Mn^{2+} allowed us to correlate the injection site in histologic sections with MR images of the same individuals. Imaging by combined phase and fluorescent microscopy of unstained gelatin-embedded sections of brains fixed immediately after acquisition of the last MR image (24 hr) identified the precise location of the injection (Fig. 2). In animals fixed 6 days after injection, no needle track or tissue damage at the injection sites were identified.

Comparison of MR images captured 0.5 hr after injection demonstrated that the injection position was accurately and reproducibly placed in all the mice studied (Fig. 3). The epicenter of the injection site ($\pm 200 \mu m$ diameter), containing the highest concentration of Mn^{2+} , appears hypointense (dark) in MR images at this early time point because the level of Mn^{2+} there was sufficient to produce significant T_2 -shortening and concomitant darkening (Lee, 1991). Analysis of the 3D location of this epicenter in each of the 13 animals demonstrated that among all animals injections were routinely placed in CA3 of the hippocampus (see Materials and Methods).

At 0.5 hr post injection, the hypointense injection site was surrounded by a white halo of hyperintensity indicating passive diffusion of the Mn^{2+} ion outward from the injection site. The halo volume was found to be $9.3 \pm 1.9 \mu l$ for the Ts65Dn cohort and $9.0 \pm 1.4 \mu l$ for the 2N littermates. An equivalent spherical volume would have a radius of 1.3 mm. Such diffusion is a common factor in all studies employing water-soluble low molecular weight tracers. Previous studies in the songbird, mouse, rat, minipig, and macaque note the same initial Mn^{2+} diffusion with no lack of specificity of subsequent projection patterns (Saleem et al., 2002, Van der Linden et al., 2002, Leergaard et al., 2003, Pautler et al., 2003, Van der Linden et al., 2004, Watanabe et al., 2004b, Jelsing et al., 2006, Murayama et al., 2006). Presumably, only

neurons in the immediate vicinity of the high Mn^{2+} concentration take up enough Mn^{2+} for detection after transport to distant sites. To focus the high concentration of Mn^{2+} in as small a brain region as possible, the volume of Mn^{2+} injected in this study (4.3 nl) was 10-1000 times less than that employed in previous studies. The reproducible placement of the injection sites and the comparable size of the diffusion halo argue that consistent amounts of both tracers, Mn^{2+} and RDA, were delivered to the same population of neurons in each animal tested. Thus, comparisons between individual animals or across cohorts are not confounded by effects due to different amounts of tracer introduced or different locations being probed.

Histological tract tracing demonstrated that the injection site was appropriate for uptake into the hippocampal-forebrain circuit

Co-injection of RDA with the Mn^{2+} allowed tracing of fluorescence in histologic sections of the same animals imaged by MR (Fig. 4). By comparing the patterns of distribution of Mn^{2+} and RDA, we confirmed that the placement of the injection site was appropriate for entry of tracer into the hippocampal-septal connections, and that the transport within those connections was operational. Small RDA such as the 3kD used here are taken up and moved inside neuronal processes, either diffusively or primarily in the retrograde direction at slow rates. Diffusive motion of small dextrans is observed in the squid axon (Terasaki et al., 1995) and 1-3 weeks is required for studies of CNS pathways in adult rodents (Reiner et al., 2000, Van Haeften and Wouterlood, 2000). In serial sections of brains fixed 6 days after injection, RDA was found along the fimbria and fornix ipsilateral to the injection site but not detectable on the contralateral, non-injected, side (Fig. 4A-C). At the level of the medial septal nucleus, containing the cholinergic neurons that send processes to the hippocampus, RDA fluorescence appeared on both sides of the midline (Fig. 4D).

These results confirm that the injection site in the hippocampus was positioned appropriately for entry into the hippocampal-septal pathway. No other locus with detectible accumulation of RDA was found. These results did not reveal any obvious difference in RDA fluorescence between DS mice and their 2N littermates in the fimbria, fornix or septal region. This is consistent with reports of another retrograde tracer, Fluorogold, which was injected in CA3 of the hippocampus in much higher quantities than in our study, and arrived into the MSN of Ts65Dn and their littermates in similar amounts (Salehi et al., 2006).

Mn^{2+} enhanced signal appears in the septal region within 6 hours of injection

Qualitative assessment of MR slices taken at the level of the basal forebrain revealed a time-dependent accumulation of Mn^{2+} in the septal nuclei after injection into the hippocampus (Fig. 5). These coronal slices were selected from 3D MR images at Bregma +0.4 mm position (see Fig. 5A for diagram). In these averaged 3D images at 0.5 hr post-injection, no Mn^{2+} enhanced brightness was seen in the septal region although slices through the injection site at Bregma -4.0 mm display Mn^{2+} enhancement as shown in Fig. 3. In contrast, by 6 hr the septal region ipsilateral to the injection site appeared brighter and this persisted in the 24 hr image (Fig 5B). Mn^{2+} enhancement in the septal region at 6 and 24 hr is qualitatively similar or greater in Ts65n mice than in 2N littermates. Mn^{2+} enhanced signal also appeared in the contralateral hippocampus at 24 hr as shown in coronal slices at the level of the dentate gyrus of the hippocampus, Bregma -2.7 (Fig. 6). Again this enhancement was qualitatively similar or greater in Ts65Dn than in 2N littermates.

Thus, Mn^{2+} was transported from the injection site in the hippocampus to the septum in relatively short times and to the contralateral hippocampus within 24 hours. Transport from the injection site to the septum required more than 0.5 hr and less than 6 hr to traverse the distance of ~6.5 mm (from injection site, along the fimbria, to septum); we thus calculate a

transport rate from 0.3 to 3.6 $\mu\text{m}/\text{sec}$, consistent with fast axonal transport of 0.05-2 $\mu\text{m}/\text{sec}$ (Satpute-Krishnan et al., 2006).

Mn²⁺ is transported further faster in Ts65Dn mice than in normal littermates

SPM along with spatial realignment and normalization have become standard methodologies for human brain imaging studies (Thompson and Toga, 1996, Thompson et al., 1997, Woods et al., 1998, Hajnal et al., 2001, Toga and Thompson, 2001, Toga and Mazziotta, 2002, Lancaster et al., 2003, Yoo, 2004). The same general procedures employed here have been used to make 'standard atlas' spaces for mouse brains of various strains and ages (MacKenzie-Graham et al., 2004, Kovacevic et al., 2005, Lee et al., 2005). Despite significant anatomical abnormalities (Baxter et al., 2000; Kurt et al., 2000; Olson et al., 2004), the brains of the Ts65Dn mice were surprisingly similar structurally, and could be aligned into the same 3D space. However, these Ts65Dn abnormalities precluded alignment of the mutant brains into the same template as their anatomically normal littermate controls. We therefore pursued analysis of the circuits enhanced by Mn²⁺ within each cohort and compared the resulting patterns between groups.

To identify dynamic changes in the anatomical pattern of Mn²⁺ enhancement over time after injection, we used SPM to compare each subsequent dataset with that immediately preceding it in the time series. Here we present three comparisons for each genotype: 0.5 hr post-injection versus pre-injection (Fig. 7A), 6 hr versus 0.5 hr (Fig. 7B), and 24 versus 6 hr post-injection (Fig. 7C). Those voxels with significantly ($P < 0.0005$) increased signal intensity in the later time point image are displayed as a colored voxel on the maps (Fig. 7).

In the 0.5 hr versus pre-injection comparisons (Fig. 7A), both sets of animals displayed similar paired Student's t-test maps at $P < 0.0005$. The injection site was in a similar position and of a similar size in the posterior hippocampus in both cohorts. This result confirms the precise position of the injection site and that the amount of Mn²⁺ injected was similar in all animals. Relative lack of enhanced signal (colored voxels in Fig. 7A) outside the injection site attests to the dependence of signal enhancement (at $P < 0.0005$) on the presence of Mn²⁺ and to the accuracy of the alignment.

Comparison of 6 hr versus 0.5 hr statistical maps demonstrated that Mn²⁺ followed the expected route from the hippocampus through the fimbria to the basal forebrain in both DS and 2N littermates (Fig. 7B). Voxels with statistically significant increased intensity were seen in both normal and Ts65Dn cohorts in CA3, the fimbria (fi), the septofimbrial nucleus (Sfi), and the LSN (Table 1). In the DS cohort more statistically significant voxels were found in these structures and significant signal had progressed further along the expected pathways, appearing already at 6 hours in the MSN, contralateral fimbria, as well as secondary olfactory structures (dorsal portion of acumbens core, anterior olfactory nucleus, and dorsal tenia tecta; see Table 1).

Continued transport in these living mice during the 6 hr to 24 hr interval was revealed by SPM comparisons of these two time points. In this case, only voxels whose intensity increased between 6 hr and 24 hr are displayed (Fig. 7C). This comparison revealed that, by 24 hr in 2N littermates, Mn²⁺ transport caught up to that seen at earlier time points in DS mice. Thus by 24 hr Mn²⁺ had progressed into the MSN in both sets of animals. By this time, both cohorts also displayed voxels with significantly increased intensity in CA3 of the contralateral hippocampus, and bed of nucleus stria terminalis (Table 1).

In addition, at 24 hr post-injection, the DS group again out-performed their 2N littermates, displaying Mn²⁺ signal further rostrally along the hippocampal-forebrain pathway, with statistically significant signal enhancement in the nucleus accumbens and areas within the ventral pallidum; the ventromedial hypothalamus and the amygdala; and the anterior part of

retrosplenial granular cortex (Fig. 7C and Table 1). Thus DS mice compared to 2N littermates displayed voxels with statistically significant Mn^{2+} enhancement further along the hippocampal-forebrain pathway at both 6 and 24 hr after injection.

Mn^{2+} enhanced signal occupies more volume along the hippocampal-forebrain tract in DS mice than in littermates

Comparison of the total volume occupied by significantly enhanced voxels ($P < 0.0005$) in the statistical parametric maps of each set of animals demonstrated that DS had a larger volume enhanced by Mn^{2+} than their 2N littermates (Fig. 8). In the map comparing the 6 hr to 0.5 hr data (Fig. 7B), the volume of Mn^{2+} enhanced voxels in the basal forebrain occupied 2.4 mm^3 in DS animals, but only 1.3 mm^3 in 2N littermates. Mn^{2+} enhanced volumes at 24 hr in the contralateral hippocampus were 3.1 mm^3 and 0.2 mm^3 in the DS and 2N littermates, respectively. Thus, the extent of Mn^{2+} transport is greater (observed further along expected tracts) and more robust (more volume affected) in DS mice as compared to 2N littermates.

Discussion

Here we show that Mn^{2+} injected into CA3 of the hippocampus dynamically traces the hippocampal to septum pathway during the 24 hours after injection. Transport of Mn^{2+} from hippocampus to basal forebrain is more robust in a trisomic mouse model of Down syndrome, Ts65Dn, than in 2N littermates. The transport pattern of Mn^{2+} enhancement measured in live animals coincides with the pattern of a coinjected traditional tracer (RDA) measured in histological sections. Histological examination revealed the typical DS phenotype of the DS mice and little to no tissue damage by the injection was observed. Alignment and averaging of MR images demonstrated the reliability of location and amount of injectate. Voxel-wise paired Student's *t*-test analysis of co-registered brain images from 7 individual DS mice at different times after injection revealed an unbiased comprehensive view of the time-course and pattern of Mn^{2+} transport. Comparisons of SPM analyses of DS mice with 2N littermates revealed that Mn^{2+} induced signal enhancement occupied more voxels and progressed more quickly along expected pathways in Ts65Dn mice than in normal 2N littermates.

Manganese as a track tracer:

Mn^{2+} , a calcium analogue, enters neurons and other cells through calcium and/or other divalent ion channels (Merritt et al., 1989, Kwan and Putney, 1990, Fasolato et al., 1993, McColl and Naccache, 1997) and is transported along neuronal pathways, even crossing synapses (Lin and Koretsky, 1997, Pautler et al., 1999, Duong et al., 2000, Leergaard et al., 2003, Watanabe et al., 2004a). Transport of Mn^{2+} is microtubule-dependent and primarily in the anterograde direction (Sloot and Gramsbergen, 1994, Tjalve et al., 1995, Pautler et al., 1998) at speeds consistent with fast axonal transport, suggesting that once in the cytoplasm, Mn^{2+} enters membrane-bound organelles and is trafficked by normal vesicular transport mechanisms. Mn^{2+} tract tracing has been used to reveal changes in neuronal circuitry in the songbird in response to endocrine stimulation (Van der Linden et al., 2002, Van der Linden et al., 2004).

The degree of Mn^{2+} induced hyperintensity at a location distant from its initial placement is dependent on at least three factors: 1) local uptake; 2) directed movement along/within the neuronal connections (including initial packaging in the cytoplasm, microtubule-based movement within processes, and possibly crossing synapses); and 3) accumulation at the distant site. Operationally we use the term "transport" to encompass all three factors. Thus, changes in transport (as evidenced by a greater or lesser amount of tracer found at the distant site) can be due to modulation of any or all of these factors. Similar caveats pertain to all tract tracers (*e.g.* radioactive or fluorescent) used to study neuronal projections. In addition to

transport defects, DS mice may also have synaptic alterations that could effect Mn^{2+} uptake (Schuchmann et al., 1998, Belichenko et al., 2004).

Retrograde versus anterograde transport:

The hippocampal to forebrain pathway contains neuronal processes emanating from either end. In each type of neuron, both anterograde and retrograde transport carry endogenous cargo to and from the cell bodies. Introduction of a traceable compound at one end of the circuit results in its transport to the other end by either anterograde or retrograde intraneuronal trafficking. Transport of NGF from the hippocampus to the basal forebrain is decreased in Down syndrome mice of the same age as those used in this work (Cooper et al., 2001, Salehi et al., 2003). This decrease is thought to be within cholinergic neurons whose cell bodies are in the MSN. Thus, decreased delivery of NGF from an injection site in the hippocampus to the septum likely reflects defects in local uptake and/or retrograde transport in these neurons. Our results suggest that this decrease may be selective for NGF transport and not a result of generalized transport deficits, since Mn^{2+} transport is at least as robust as in normal littermates. In support of this, retrograde transport of Fluorogold, also a general tracer for retrograde connections, is also apparently normal in these mice, although more difficult to quantify precisely (Salehi et al., 2006).

In vivo Mn^{2+} enhanced MRI allows quantitative analysis of transport dynamics in living animals:

MR imaging provided three advantages over traditional approaches to the study of transport in the hippocampal to forebrain pathway. First, live animals could be imaged repeatedly, thereby obtaining a sequential view of the process of transport along the pathway. Second, three dimensional information is obtained in a holistic image acquired in one session, avoiding the artifacts of fixation, embedding and sectioning and speeding data collection. Third, quantitative analysis of pooled samples allows statistical significance across a cohort of individuals to be obtained. Thus, more reliable information from living animals in three dimensions with statistical power is possible with MRI.

SPM provides a comprehensive anatomically unbiased view of the time dependence of Mn^{2+} transport in the DS and normal mice. This approach revealed that the entire pathway from the hippocampus to the basal forebrain was enhanced at 6 hr compared to 0.5 hr post-injection. The volume of enhancement in the basal forebrain was almost a factor of two larger in trisomic versus normal animals; directly confirming the more robust character of transport in this Down syndrome model. At 24 hr compared to 6 hr post-injection, the volume of enhancement in the contralateral hippocampus is a factor of 12 larger in DS mice than normal animals. Thus, these observations depict an overall increase in transport efficacy in the DS mice, which also extends beyond the hippocampal to basal forebrain circuit to more distal locations.

Axonal transport in neurological disease:

Evidence is accumulating that axonal transport plays a significant role in neuronal survival and neurodegenerative diseases (Mandelkow et al., 2004, Morfini et al., 2005, Stokin et al., 2005, Chevalier-Larsen and Holzbaur, 2006). Four mechanisms underlying altered transport have been proposed (Goldstein, 2003, Salehi et al., 2004, Morfini et al., 2005): (1) blockage of the path, (2) abnormal tracks, (3) defects in motor machinery, and (4) disrupted signaling. Physical blockage of the axon lumen would hamper transport in both directions, as would disruption of microtubule tracks or general motor defects. We thus exclude these three possibilities as mechanisms to explain decreased transport of NGF in these mice, since we observed more robust transport of Mn^{2+} in the DS mouse model, while retrograde transport of low molecular weight RDA and Fluorogold transport both appear unchanged (Salehi et al.,

2006). Secondly, both anterograde and retrograde motors (kinesin and dynein) use the same microtubule track system, thus a general destabilization of tracks is inconsistent with current observations concerning transport in the DS model. Our results do not rule out a selective defect in NGF transport that may involve a defect in uptake, binding/linkage of NGF-bearing cargo to the motor or signals that activate its transport.

Another plausible explanation for both more robust anterograde and selectively decreased retrograde transport in DS mice could be that high APP levels increase affinity of transport vesicles for anterograde motors at the expense of retrograde motors, thus altering the balance between anterograde and retrograde transport (Salehi et al., 2006). Among the genes that are triplicated in human Down syndrome is amyloid precursor protein (APP), a component of senile plaques of Alzheimer's disease and recently implicated as a vesicular receptor for axonal motor machinery (Satpute-Krishnan et al., 2006, Kamal et al., 2000, Kamal, 2001, Lazarov et al., 2005). APP is among the genes that co-segregates with mental retardation in partial trisomies in human (Korenberg et al., 1994). Ts65Dn mice also carry three copies of the APP gene and over-express the protein (Salehi et al., 2006, Seregaza et al., 2006). The necessary coordination of anterograde and retrograde transport (Martin et al., 1999, Gross et al., 2002, Welte, 2004, Klumpp and Lipowsky, 2005) implies that effective movement of cargo (e.g. NGF) could be disrupted without altering the detailed molecular mechanisms involved in movement along tracks, but simply by disrupting the interaction(s) that coordinate directionality.

Conclusion:

The use of Mn^{2+} as a transport tracer and longitudinal magnetic resonance imaging allowed us to measure transport dynamics *in vivo* in individual animals. This revealed functional differences in the hippocampal to forebrain pathway in a mouse model of Down syndrome. Co-registration of images from a cohort of animals allows application of statistical methods for unbiased evaluation of spatio-temporal changes in Mn^{2+} transport, revealing more robust transport in the Down syndrome mouse. No other technology offers the ability to peer into the living mammalian brain and determine physiological transport parameters. These results point out that neuronal transport is a complicated phenomenon and that alterations in transport dynamics can have important ramifications in cognitive functioning. Future application of this powerful technology to earlier stages in DS and to other types of neuropathologies where transport defects are implicated will undoubtedly provide more mechanistic insights.

Acknowledgements:

We thank Muriel Davisson and Cecilia Schmidt for their advice and help in obtaining and genotyping aged Ts65Dn mice and 2N littermates, to J.D. DelCroix for advice on hippocampal injections, and to the Moore Foundation for the Moore Distinguished Scholar award that brought E.L.B. to Caltech to collaborate in this work. The project was in part funded by NINDS NS046810, NIGMS GM47368 (E.L.B.), NCRR U24 RR021760 entitled Mouse BIRN and NIDA R01DA018184 (R.E.J.).

Abbreviations:

RDA, 3kD rhodamine-dextran-amine; MSN, medial septal nuclei; LSN, lateral septal nuclei; MoDG, molecular layer of the dentate gyrus; S, subiculum.

References

Alonso JR, U HS, Amaral DG. Cholinergic innervation of the primate hippocampal formation: II. Effects of fimbria/fornix transection. *J Comp Neurol* 1996;375:527–551. [PubMed: 8930785]

- Amaral DG, Kurz J. An Analysis of the Origins of the Cholinergic and Noncholinergic Septal Projections to the Hippocampal-Formation of the Rat. *Journal of Comparative Neurology* 1985;240:37–59. [PubMed: 4056104]
- Bearer EL, Breakefield XO, Schuback D, Reese TS, LaVail JH. Retrograde axonal transport of herpes simplex virus: evidence for a single mechanism and a role for tegument. *Proc Natl Acad Sci U S A* 2000;97:8146–8150. [PubMed: 10884436]
- Belichenko PV, Masliah E, Kleschevnikov AM, Villar AJ, Epstein CJ, Salehi A, Mobley WC. Synaptic structural abnormalities in the Ts65Dn mouse model of Down Syndrome. *J Comp Neurol* 2004;480:281–298. [PubMed: 15515178]
- Chevalier-Larsen E, Holzbaur ELF. Axonal transport and neurodegenerative disease. *Biochimica et Biophysica Acta (BBA) - Molecular Basis of Disease* 2006;1762:1094–1108.
- Colom LV. Septal networks: relevance to theta rhythm, epilepsy and Alzheimer's disease. *Journal of Neurochemistry* 2006;96:609–623. [PubMed: 16405497]
- Cooper JD, Salehi A, Delcroix JD, Howe CL, Belichenko PV, Chua-Couzens J, Kilbridge JF, Carlson EJ, Epstein CJ, Mobley WC. Failed retrograde transport of NGF in a mouse model of Down's syndrome: reversal of cholinergic neurodegenerative phenotypes following NGF infusion. *Proc Natl Acad Sci U S A* 2001;98:10439–10444. [PubMed: 11504920]
- Cross DJ, Minoshima S, Anzai Y, Flexman JA, Keogh BP, Kim Y, Maravilla KR. Statistical mapping of functional olfactory connections of the rat brain in vivo. *NeuroImage* 2004;23:1326–1335. [PubMed: 15589097]
- Davissou MT, Schmidt C, Akeson EC. Segmental trisomy of murine chromosome 16: a new model system for studying Down syndrome. *Prog Clin Biol Res* 1990;360:263–280. [PubMed: 2147289]
- Davissou MT, Schmidt C, Reeves RH, Irving NG, Akeson EC, Harris BS, Bronson RT. Segmental trisomy as a mouse model for Down syndrome. *Prog Clin Biol Res* 1993;384:117–133. [PubMed: 8115398]
- Delcroix JD, Valletta J, Wu C, Howe CL, Lai CF, Cooper JD, Belichenko PV, Salehi A, Mobley WC. Trafficking the NGF signal: implications for normal and degenerating neurons. *Prog Brain Res* 2004;146:3–23. [PubMed: 14699953]
- Duong TQ, Silva AC, Lee SP, Kim SG. Functional MRI of calcium-dependent synaptic activity: Cross correlation with CBF and BOLD measurements. *Magn Reson Med* 2000;43:383–392. [PubMed: 10725881]
- Epstein, CJ. *Consequences of Chromosomal Imbalanc: Principals, Mechanisms and Models*. Cambridge University PRes; New York: 1986.
- Fasolato C, Hoth M, Matthews G, Penner R. Ca²⁺ and Mn²⁺ influx through receptor-mediated activation of nonspecific cation channels in mast cells. *Proc Natl Acad Sci U S A* 1993;90:3068–3072. [PubMed: 7681994]
- Gaykema RP, van der Kuil J, Hersh LB, Luiten PG. Patterns of direct projections from the hippocampus to the medial septum-diagonal band complex: anterograde tracing with Phaseolus vulgaris leucoagglutinin combined with immunohistochemistry of choline acetyltransferase. *Neuroscience* 1991;43:349–360. [PubMed: 1656317]
- Goldstein LSB. Do Disorders of Movement Cause Movement Disorders and Dementia? *Neuron* 2003;40:415–425. [PubMed: 14556718]
- Granhholm AC, Sanders LA, Crnic LS. Loss of cholinergic phenotype in basal forebrain coincides with cognitive decline in a mouse model of Down's syndrome. *Exp Neurol* 2000;161:647–663. [PubMed: 10686084]
- Gross SP, Welte MA, Block SM, Wieschaus EF. Coordination of opposite-polarity microtubule motors. *J Cell Biol* 2002;156:715–724. [PubMed: 11854311]
- Hajnal, JV.; Hill, DLG.; Hawkes, DJ. *Medical Image Registration*. CRC Press; Boca Raton, FL.: 2001.
- Hennig J, Nauwerth A, Friedburg H. RARE imaging: a fast imaging method for clinical MR. *Magn Reson Med* 1986;3:823–833. [PubMed: 3821461]
- Hof, PR.; Bloom, FE.; Belichenko, PV.; Celio, MR. *Comparative Cytoarchitectonic Atlas of the C57bl/6 and 129/SV Mouse Brains*. Elsevier; New York: 2000.
- Holtzman DM, Santucci D, Kilbridge J, Chua-Couzens J, Fontana DJ, Daniels SE, Johnson RM, Chen K, Sun Y, Carlson E, Alleve E, Epstein CJ, Mobley WC. Developmental abnormalities and age-

- related neurodegeneration in a mouse model of Down syndrome. *Proc Natl Acad Sci U S A* 1996;93:13333–13338. [PubMed: 8917591]
- Hunter CL, Isacson O, Nelson M, Bimonte-Nelson H, Seo H, Lin L, Ford K, Kindy MS, Granholm AC. Regional alterations in amyloid precursor protein and nerve growth factor across age in a mouse model of Down's syndrome. *Neurosci Res* 2003;45:437–445. [PubMed: 12657457]
- Jaffe LA, Terasaki M. Quantitative microinjection of oocytes, eggs, and embryos. *Methods Cell Biol* 2004;74:219–242. [PubMed: 15575609]
- Jelsing J, Hay-Schmidt A, Dyrby T, Hemmingsen R, Uylings HBM, Pakkenberg B. The prefrontal cortex in the Gottingen minipig brain defined by neural projection criteria and cytoarchitecture. *Brain Research Bulletin* 2006;70:322–336. [PubMed: 17027768]
- Klumpp S, Lipowsky R. Cooperative cargo transport by several molecular motors. *PNAS* 2005;102:17284–17289. [PubMed: 16287974]
- Korenberg JR, Chen X, Schipper R, Sun Z, Gonsky R, Gerwehr S, Carpenter N, Daumer C, Dignan P, Disteche C, Graham JM Jr, Hudgins L, McGillivray B, Miyazaki K, Ogasawara N, Park JP, Pagon R, Pueschel S, Sack G, Say B, Schuffenhauer S, Soukup S, Yamanaka T. Down Syndrome Phenotypes: The Consequences of Chromosomal Imbalance. *PNAS* 1994;91:4997–5001. [PubMed: 8197171]
- Kovacevic N, Henderson JT, Chan E, Lifshitz N, Bishop J, Evans AC, Henkelman RM, Chen XJ. A Three-dimensional MRI Atlas of the Mouse Brain with Estimates of the Average and Variability. *Cereb Cortex* 2005;15:639–645. [PubMed: 15342433]
- Kwan CY, Putney JW Jr. Uptake and intracellular sequestration of divalent cations in resting and methacholine-stimulated mouse lacrimal acinar cells. Dissociation by Sr²⁺ and Ba²⁺ of agonist-stimulated divalent cation entry from the refilling of the agonist-sensitive intracellular pool. *J Biol Chem* 1990;265:678–684. [PubMed: 2404009]
- Lancaster JL, Kochunov PV, Thompson PM, Toga AW, Fox PT. Asymmetry of the brain surface from deformation field analysis. *Human Brain Mapping* 2003;19:79–89. [PubMed: 12768532]
- Lee DH. Mechanisms of contrast enhancement in magnetic resonance imaging. *Can Assoc Radiol J* 1991;42:6–12. [PubMed: 2001531]
- Lee E-F, Jacobs RE, Dinov I, Loew A, Toga AW. Standard atlas space for C57BL/6J neonatal mouse brain. *Anat Embryol* 2005;210:245–263. [PubMed: 16228227]
- Leergaard TB, Bjaalie JG, Devor A, Wald LL, Dale AM. In vivo tracing of major rat brain pathways using manganese-enhanced magnetic resonance imaging and three-dimensional digital atlas. *Neuroimage* 2003;20:1591–1600. [PubMed: 14642470]
- Lin YJ, Koretsky AP. Manganese ion enhances T1-weighted MRI during brain activation: an approach to direct imaging of brain function. *Magn Reson Med* 1997;38:378–388. [PubMed: 9339438]
- Liu DP, Schmidt C, Billings T, Davisson MT. Quantitative PCR genotyping assay for the Ts65Dn mouse model of Down syndrome. *BioTechniques* 2003;35:1170–1174. [PubMed: 14682051]
- MacKenzie-Graham A, Lee E-F, Dinov ID, Bota M, Shattuck DW, Ruffins S, Yuan H, Konstantinidis F, Pitiot A, Ding Y, Hu G, Jacobs RE, Toga AW. A multimodal, multidimensional atlas of the C57BL/6J mouse brain. *J Anatomy* 2004;204:93–102.
- Mandelkow E-M, Thies E, Trinczek B, Biernat J, Mandelkow E. MARK/PAR1 kinase is a regulator of microtubule-dependent transport in axons. *J Cell Biol* 2004;167:99–110. [PubMed: 15466480]
- Martin M, Iyadurai SJ, Gassman A, Gindhart JG Jr, Hays TS, Saxton WM. Cytoplasmic Dynein, the Dynactin Complex, and Kinesin Are Interdependent and Essential for Fast Axonal Transport. *Mol Biol Cell* 1999;10:3717–3728. [PubMed: 10564267]
- McCull SR, Naccache PH. Calcium mobilization assays. *Methods Enzymol* 1997;288:301–309. [PubMed: 9357000]
- Merritt JE, Jacob R, Hallam TJ. Use of manganese to discriminate between calcium influx and mobilization from internal stores in stimulated human neutrophils. *J Biol Chem* 1989;264:1522–1527. [PubMed: 2536366]
- Morfini G, Pigino G, Brady ST. Polyglutamine expansion diseases: failing to deliver. *Trends in Molecular Medicine* 2005;11:64–70. [PubMed: 15694868]
- Murayama Y, Weber B, Saleem KS, Augath M, Logothetis NK. Tracing neural circuits in vivo with Mn-enhanced MRI. *Magnetic Resonance Imaging* 2006;24:349–358. [PubMed: 16677940]

- Olson LE, Roper RJ, Baxter LL, Carlson EJ, Epstein CJ, Reeves RH. Down syndrome mouse models Ts65Dn, Ts1Cje, and Ms1Cje/Ts65Dn exhibit variable severity of cerebellar phenotypes. *Developmental Dynamics* 2004;230:581–589. [PubMed: 15188443]
- Pautler R, Olson C, Williams D, Ho C, Koretsky A. In Vivo Tract Tracing using Manganese Enhanced MRI (MEMRI) in Mouse Mutants and Non-human Primates. *Proc Intl Soc Mag Reson Med* 1999;7:448.
- Pautler RG, Mongeau R, Jacobs RE. In vivo trans-synaptic tract tracing from the murine striatum and amygdala utilizing manganese enhanced MRI (MEMRI). *Magnetic Resonance in Medicine* 2003;50:33–39. [PubMed: 12815676]
- Pautler RG, Silva AC, Koretsky AP. In vivo neuronal tract tracing using manganese-enhanced magnetic resonance imaging. *Magn Reson Med* 1998;40:740–748. [PubMed: 9797158]
- Paxinos, G.; Franklin, K. *The Mouse Brain in Stereotaxic Coordinates*. Academic Press; San Diego: 2001.
- Reeves RH, Irving NG, Moran TH, Wohn A, Kitt C, Sisodia SS, Schmidt C, Bronson RT, Davisson MT. A Mouse Model for Down-Syndrome Exhibits Learning and Behavior Deficits. *Nature Genetics* 1995;11:177–184. [PubMed: 7550346]
- Reiner A, Veenman CL, Medina L, Jiao Y, Del Mar N, Honig MG. Pathway tracing using biotinylated dextran amines. *J Neurosci Methods* 2000;103:23–37. [PubMed: 11074093]
- Risold PY, Swanson LW. Structural evidence for functional domains in the rat hippocampus. *Science* 1996;272:1484–1486. [PubMed: 8633241]
- Risold PY, Swanson LW. Connections of the rat lateral septal complex. *Brain Res Brain Res Rev* 1997;24:115–195. [PubMed: 9385454]
- Roper RJ, Reeves RH. Understanding the basis for Down syndrome phenotypes. *Plos Genetics* 2006;2:231–236.
- Rorden C, Brett M. Stereotaxic display of brain lesions. *Behavioural Neurology* 2000;12:191–200. [PubMed: 11568431]
- Saleem KS, Pauls JM, Augath M, Trinath T, Prause BA, Hashikawa T, Logothetis NK. Magnetic resonance imaging of neuronal connections in the macaque monkey. *Neuron* 2002;34:685–700. [PubMed: 12062017]
- Salehi A, Delcroix J-D, Belichenko PV, Zhan K, Wu C, Valletta JS, Takimoto-Kimura R, Kleschevnikov AM, Sambamurti K, Chung PP. Increased App Expression in a Mouse Model of Down's Syndrome Disrupts NGF Transport and Causes Cholinergic Neuron Degeneration. *Neuron* 2006;51:29–42. [PubMed: 16815330]
- Salehi A, Delcroix JD, Mobley WC. Traffic at the intersection of neurotrophic factor signaling and neurodegeneration. *Trends Neurosci* 2003;26:73–80. [PubMed: 12536130]
- Salehi A, Delcroix JD, Swaab DF. Alzheimer's Disease and NGF Signaling. *J Neural Transmission* 2004;111:323–345.
- Satpute-Krishnan P, DeGiorgis JA, Conley MP, Jang M, Bearer EL. A peptide zipcode sufficient for anterograde axonal transport within amyloid precursor protein. *Proc Natl Acad Sci U S A* 2006;103:16532–16537. [PubMed: 17062754]
- Schuchmann S, Muller W, Heinemann U. Altered Ca²⁺ signaling and mitochondrial deficiencies in hippocampal neurons of trisomy 16 mice: a model of Down's syndrome. *J Neurosci* 1998;18:7216–7231. [PubMed: 9736644]
- Seo H, Isacson O. Abnormal APP, cholinergic and cognitive function in Ts65Dn Down's model mice. *Exp Neurol* 2005;193:469–480. [PubMed: 15869949]
- Seregaza Z, Roubertoux PL, Jamon M, Soumireu-Mourat B. Mouse models of cognitive disorders in trisomy 21: a review. *Behav Genet* 2006;36:387–404. [PubMed: 16523244]
- Silva AC, Lee JH, Aoki L, Koretsky AR. Manganese-enhanced magnetic resonance imaging (MEMRI): methodological and practical considerations. *Nmr in Biomedicine* 2004;17:532–543. [PubMed: 15617052]
- Sloot WN, Gramsbergen JB. Axonal transport of manganese and its relevance to selective neurotoxicity in the rat basal ganglia. *Brain Res* 1994;657:124–132. [PubMed: 7820609]
- Stokin GB, Lillo C, Falzone TL, Brusch RG, Rockenstein E, Mount SL, Raman R, Davies P, Masliah E, Williams DS, Goldstein LS. Axonopathy and transport deficits early in the pathogenesis of Alzheimer's disease. *Science* 2005;307:1282–1288. [PubMed: 15731448]

- Terasaki M, Schmidek A, Galbraith JA, Gallant PE, Reese TS. Transport of Cytoskeletal Elements in the Squid Giant Axon. *Proc Natl Acad Sci U S A* 1995;92:11500–11503. [PubMed: 8524791]
- Thompson P, MacDonald D, Mega M, Holmes C, Evans A, Toga AW. Detection and mapping of abnormal brain structure with a probabilistic atlas of cortical surfaces. *J Comput Assist Tomogr* 1997;21:567–581. [PubMed: 9216760]
- Thompson P, Toga AW. A surface-based technique for warping three-dimensional images of the brain. *Ieee Transactions on Medical Imaging* 1996;15:402–417.
- Tjalve H, Mejare C, Borg-Neczak K. Uptake and transport of manganese in primary and secondary olfactory neurones in pike. *Pharmacol Toxicol* 1995;77:23–31. [PubMed: 8532608]
- Toga, AW.; Mazziotta, JC., editors. *Brain Mapping: The Methods*. 2nd Ed.. Academic Press; San Diego: 2002.
- Toga AW, Thompson PM. The role of image registration in brain mapping. *Image and Vision Computing* 2001;19:3–24.
- Tuszynski MH, Thal L, Pay M, Salmon DP, U HS, Bakay R, Patel P, Blesch A, Vahlsing HL, Ho G, Tong G, Potkin SG, Fallon J, Hansen L, Mufson EJ, Kordower JH, Gall C, Conner J. A phase 1 clinical trial of nerve growth factor gene therapy for Alzheimer disease. *Nat Med* 2005;11:551–555. [PubMed: 15852017]
- Tuszynski MH, U HS, Amaral DG, Gage FH. Nerve growth factor infusion in the primate brain reduces lesion-induced cholinergic neuronal degeneration. *J Neurosci* 1990;10:3604–3614. [PubMed: 2230949]
- Van der Linden A, Van Meir V, Tindemans I, Verhoye M, Balthazar J. Applications of manganese-enhanced magnetic resonance imaging (MEMRI) to image brain plasticity in song birds. *NMR in Biomedicine* 2004;17:602–612. [PubMed: 15761949]
- Van der Linden A, Verhoye M, Van Meir V, Tindemans I, Eens M, Absil P, Balthazar J. In vivo manganese-enhanced magnetic resonance imaging reveals connections and functional properties of the songbird vocal control system. *Neuroscience* 2002;112:467–474. [PubMed: 12044464]
- Van Haeften T, Wouterlood FG. Neuroanatomical tracing at high resolution. *J Neurosci Methods* 2000;103:107–116. [PubMed: 11074100]
- Watanabe T, Frahm J, Michaelis T. Functional mapping of neural pathways in rodent brain in vivo using manganese-enhanced three-dimensional magnetic resonance imaging. *NMR in Biomedicine* 2004a; 17:554–568. [PubMed: 15617054]
- Watanabe T, Radulovic J, Spiess J, Natt O, Boretius S, Frahm J, Michaelis T. In vivo 3D MRI staining of the mouse hippocampal system using intracerebral injection of MnCl₂. *Neuroimage* 2004b; 22:860–867. [PubMed: 15193616]
- Welte MA. Bidirectional Transport along Microtubules. *Current Biology* 2004;14:R525–R537. [PubMed: 15242636]
- Woods RP, Grafton ST, Holmes CJ, Cherry SR, Mazziotta JC. Automated image registration: I. General methods and intrasubject, intramodality validation. *J Comput Assist Tomogr* 1998;22:139–152. [PubMed: 9448779]
- Wu M, Shanabrough M, Leranath C, Alreja M. Cholinergic excitation of septohippocampal GABA but not cholinergic neurons: implications for learning and memory. *J Neurosci* 2000;20:3900–3908. [PubMed: 10804229]
- Yoo, TS. *Insight into Images: Principles and Practice for Segmentation, Registration, and Image Analysis*. AK Peters, Ltd.; Wellesey, MA: 2004.

Supplementary Material

Refer to Web version on PubMed Central for supplementary material.

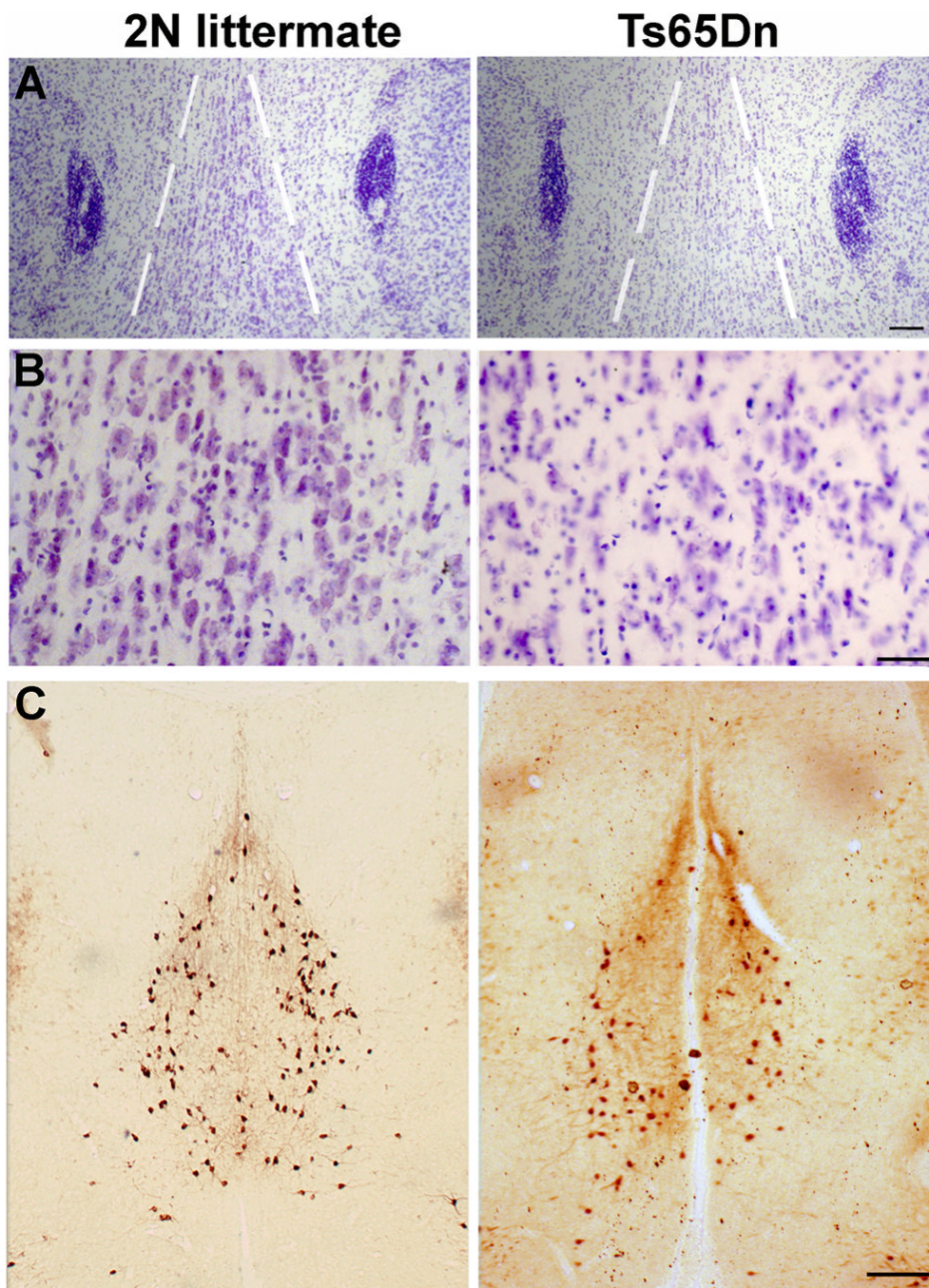


Figure 1. DS mice have fewer cholinergic neurons in the MSN

A. Examples of coronal histologic sections of Ts65Dn and 2N littermates at the level the MSN (approximately Bregma +0.4–0.5) stained with thionine-Nissl. The MSN is the A-shaped region in the center of the images indicated by dashed white lines. Note decreased cell density. Bar = 100 μ m.

B. Higher magnification of the central region of the MSNs shown in A above. Note the decreased number of cell nuclei in Ts65Dn in this region of the brain. Bar = 40 μ m.

C. Adjacent sections stained with anti-ChAT for immunohistochemistry showing decreased numbers of cholinergic neurons in the MSN of DS compared to littermates. Bar = 200 μ m.



Figure 2. Injection site visualized in histologic sections showing lack of tissue damage
Shown is an example of the injection site as imaged by light microscopy in one of the mouse brains perfusion fixed after the last MR imaging at 24 hr post-injection. In histologic sections the injection site in the hippocampus was readily identified by the red fluorescence from the co-injected RDA. Histological examination identified little tissue damage. Bar = 100 μ m.

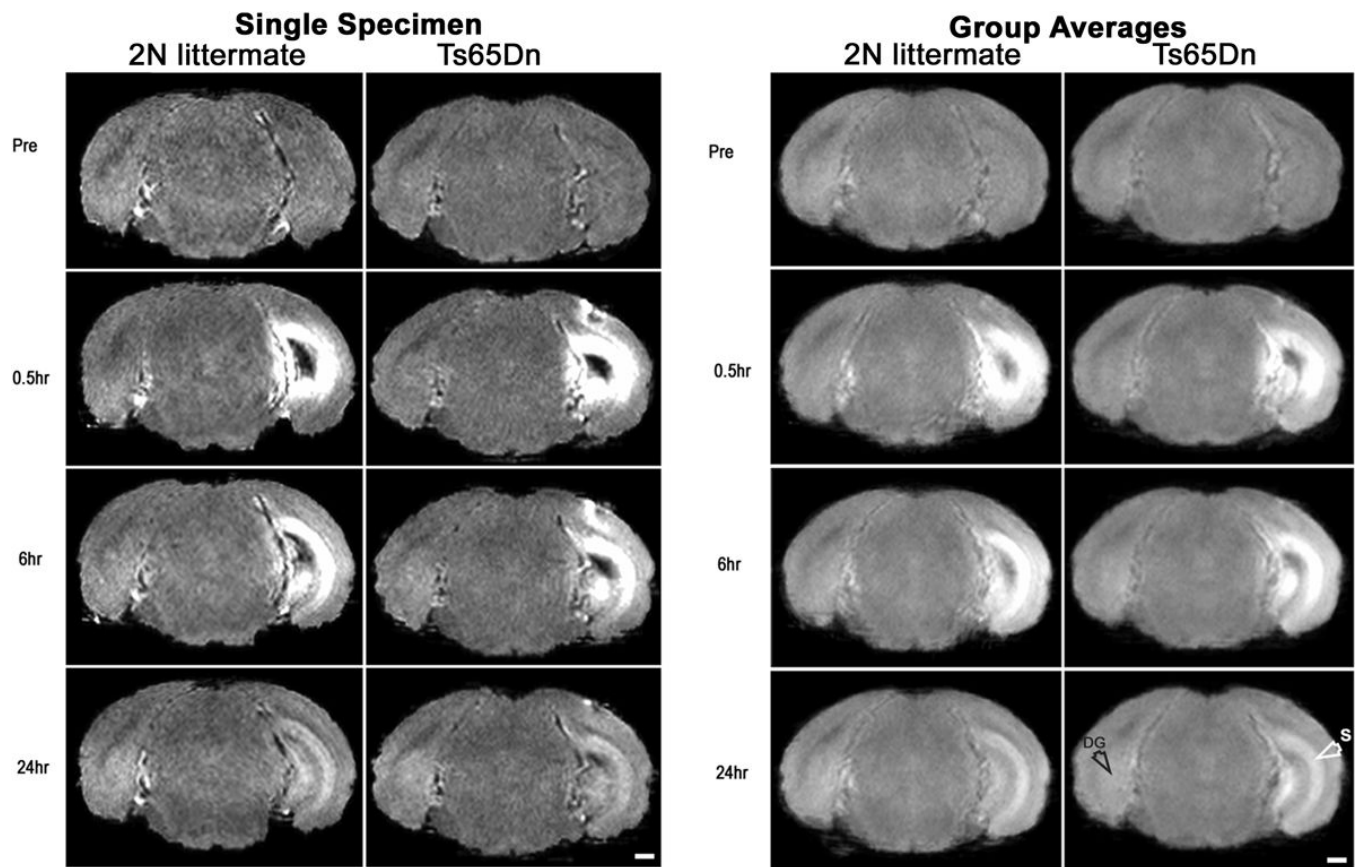


Figure 3. Consistent placement of injection determined by MRI analysis
 Coronal slices from 3D data sets showing the injection site (Bregma -4 mm) at 4 time points. Left panel show slices from a single animal in each cohort (2N normal and DS). Right panel shows the same slice taken from the averaged images at each time point. Subiculum (S, white arrowhead) and dentate gyrus (DG, black arrowhead) of the hippocampus are noted in the lower right panel. Bar = $500\mu\text{m}$.

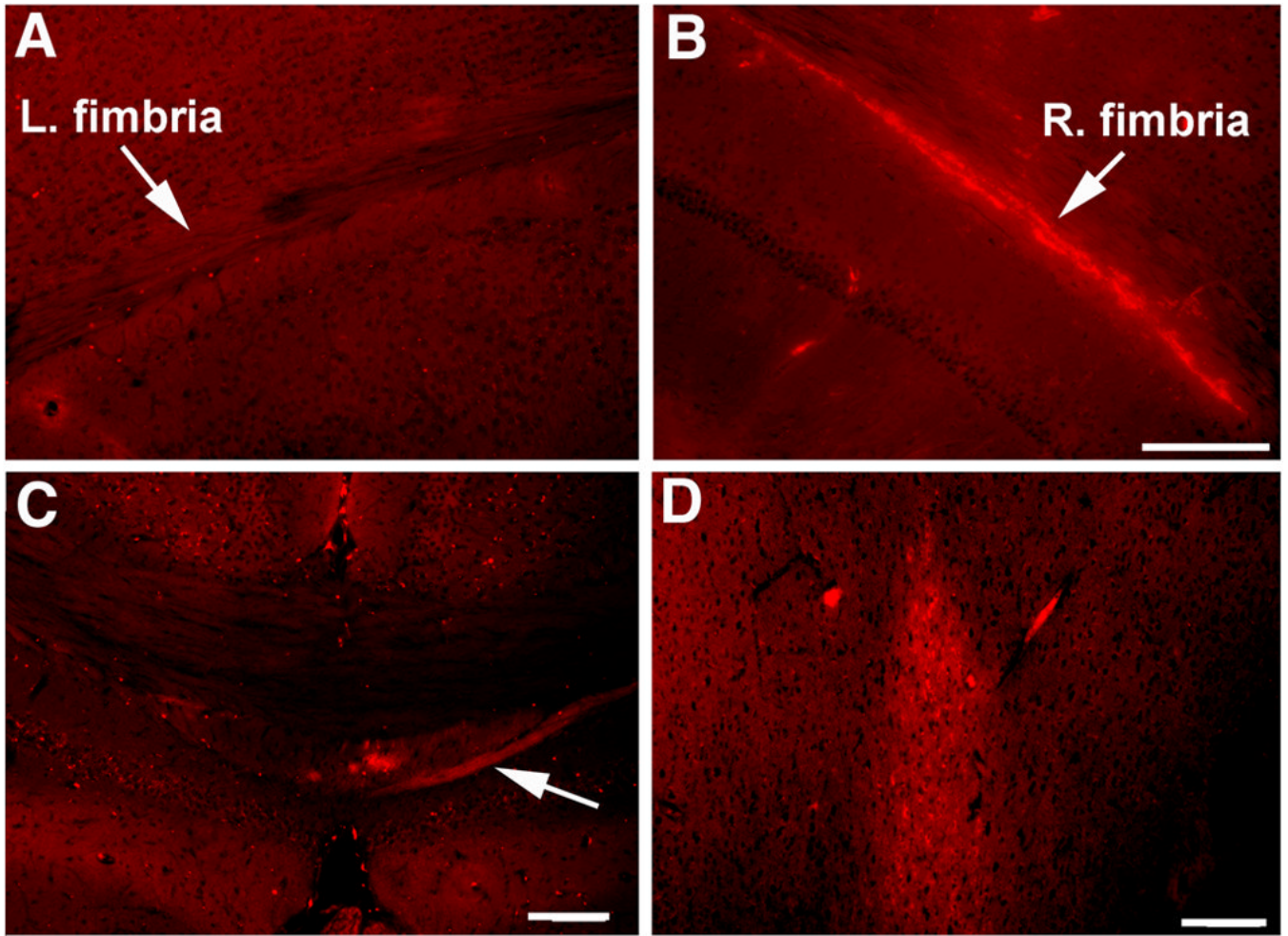


Figure 4. Transport of 3kD rhodamine-dextran-amine, a traditional tract tracer, from hippocampus to medial septum after co-injection with the Mn^{2+} into the right hippocampus
A. and B. Fluorescence microscopy of a coronal section through the hippocampus anterior to the injection site (at Bregma -2.46). The tracks exiting the hippocampus in the fimbria/alveus on the right side (B) show rhodamine fluorescence (arrows) but no fluorescence above background is seen on the uninjected left side (A). Bar = $200\ \mu m$
C. Lower magnification showing fluorescence of the RDA on the right (arrow) but not left side of the hippocampal commissure at the midline (Bregma $-1.46\ mm$) of the same mouse brain shown in A and B. Tracer is also not present in the cortical commissures, above (dorsal to) the hippocampal fibers. Bar = $200\ \mu m$
D. Medial septal nuclei (Bregma $+0.4\ mm$) also show rhodamine fluorescence indicating transport of the RDA tracer to the septum. In this example, the 2N littermate brain was fixed by perfusion 6 days after injection. Bar= $100\ \mu m$.

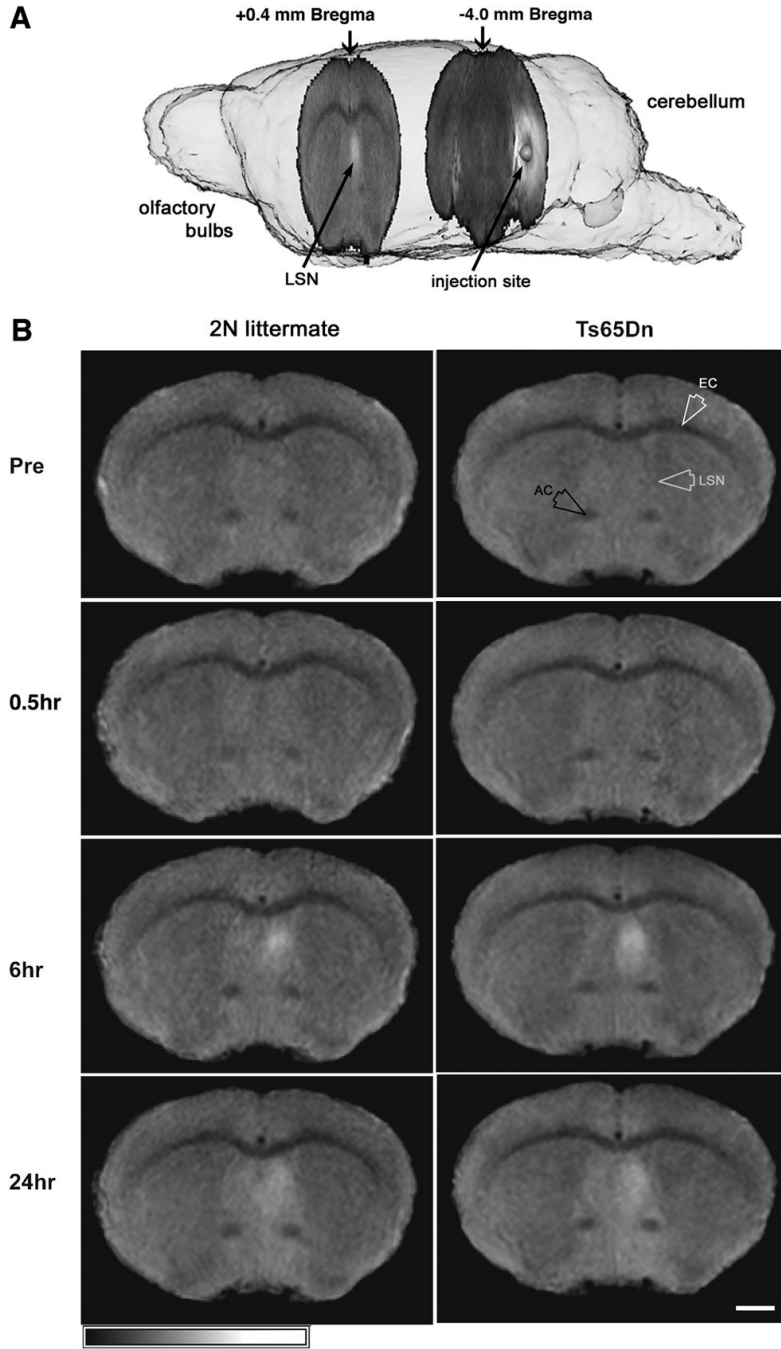


Figure 5. Mn^{2+} is transported to the forebrain at 6 hours after hippocampal injection
A. Schematic showing the positions of the injection site in the hippocampus and of the septal nuclei in the forebrain. Shown are 2 coronal slices within a semitransparent rendering of the mouse brain. The view is from the front left side of the brain, anterior to the left, posterior to the right. The slice at Bregma -4.0 mm (4 mm posterior to Bregma) is from the averaged Ts65Dn 24hr data (see Figure 3) at the level of the injection site, which is indicated by a small sphere within the hippocampus. The slice at Bregma 0.4 mm (0.4 mm anterior to Bregma) is from the averaged 6 hr Ts65Dn data (see Figure 3) where Mn^{2+} hyperintensity is clearly visible in the septal nuclei (LSN, lateral septal nuclei).

B. MRI images (coronal sections) taken from the averaged 3D datasets at the level of the septal nuclei (Bregma 0.4 mm) at 4 time points. The left panel shows slices from the 2N littermates and right panel from the trisomics. All images are at the same spatial and intensity scales and have been rendered identically. No changes are observed between the pre-injected image (top row) and 0.5 hr after injection (2nd row). By 6 hr after injection, significant hyperintensity is clearly observed in the ipsilateral LSN, which is maintained in the 24 hr image. External capsule (EC, white arrowhead), one arm of the anterior commissure (AC, black arrowhead), and LSN (gray arrowhead) are noted in the upper right panel. Bar = 1 mm.

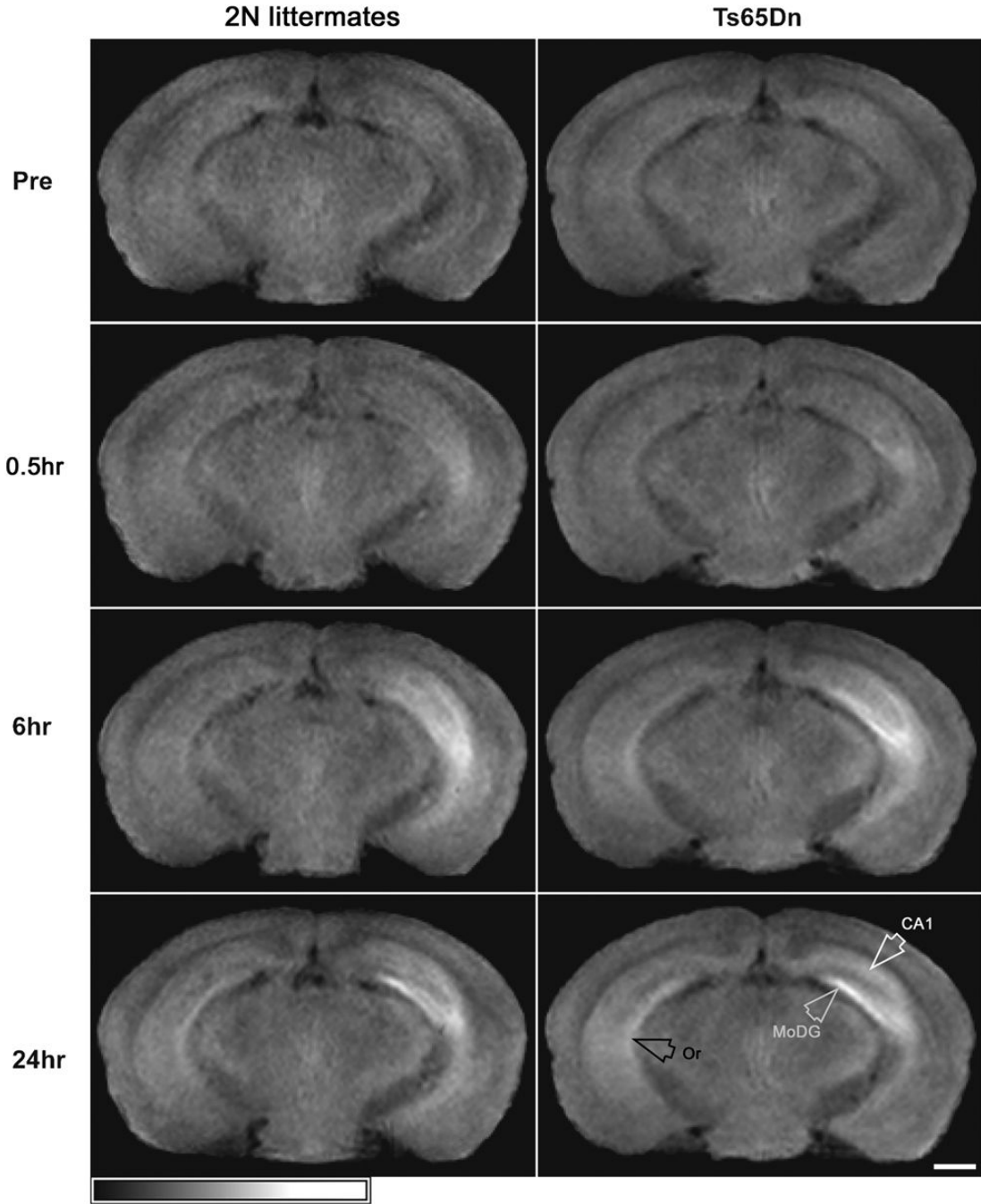


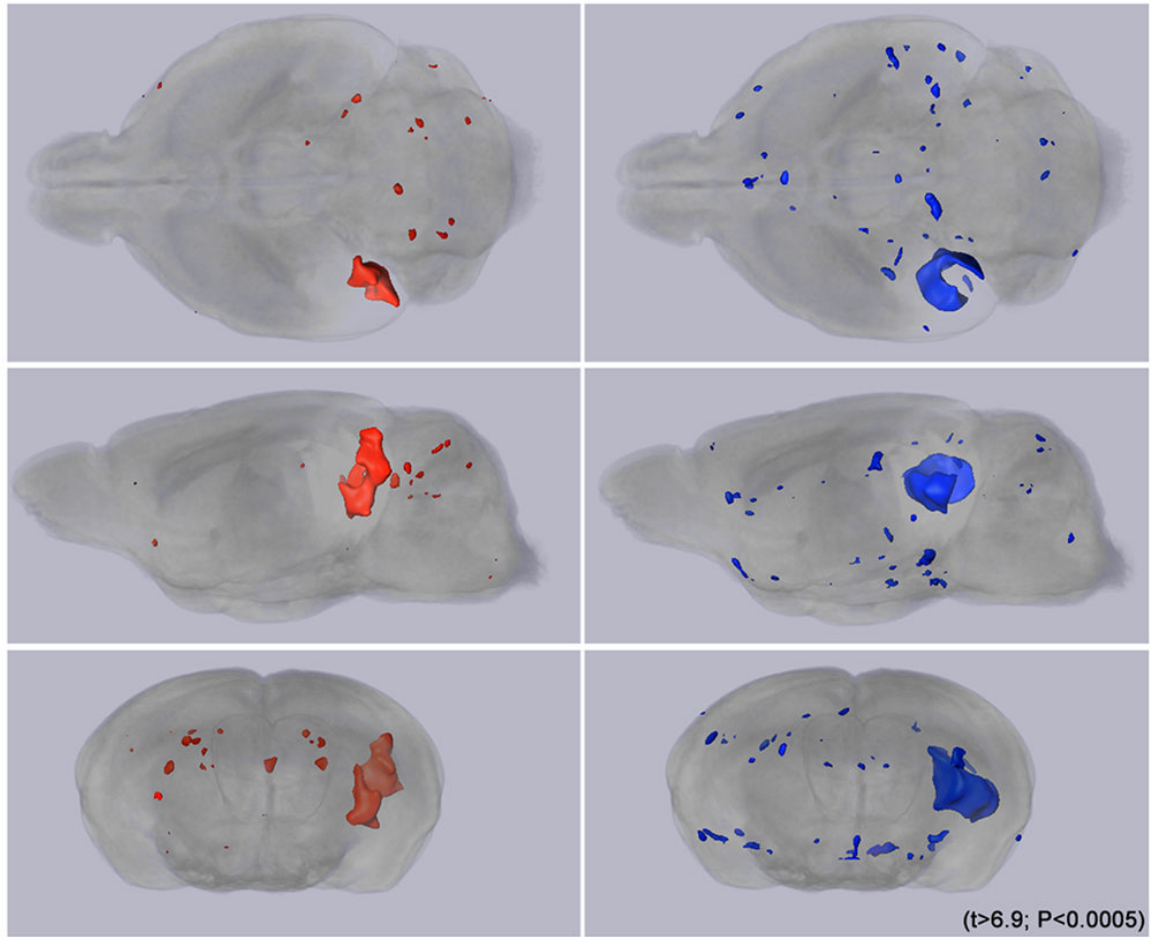
Figure 6. Mn^{2+} is transported to the contralateral hippocampus at 24 hr post-injection
 MR images (coronal slices) taken from the same averaged 3D datasets as in Figure 5 but at the level of the mid hippocampus (Bregma -2.7 mm) at the same four time points. The left panel shows slices from the 2N littermates and right panel from the trisomics (Ts65DN). All images are at the same spatial and intensity scales and have been rendered identically. By 0.5 hr after injection (2nd row) signal increases are noted in portions of CA3 ipsilateral to the injection site. By 6 hr after injection, significant hyperintensity is observed in much of the ipsilateral hippocampus, while at 24 hr signal increases are observed in the contralateral hippocampus. CA1 (white arrowhead), oriens layer (OR, black arrowhead) and molecular layer of the dentate gyrus (MoDG, gray arrowhead) are noted in the lower right panel. Bar = 1 mm.

Statistical map: 0.5 hour > preinjection

2N littermates

Ts65Dn

a

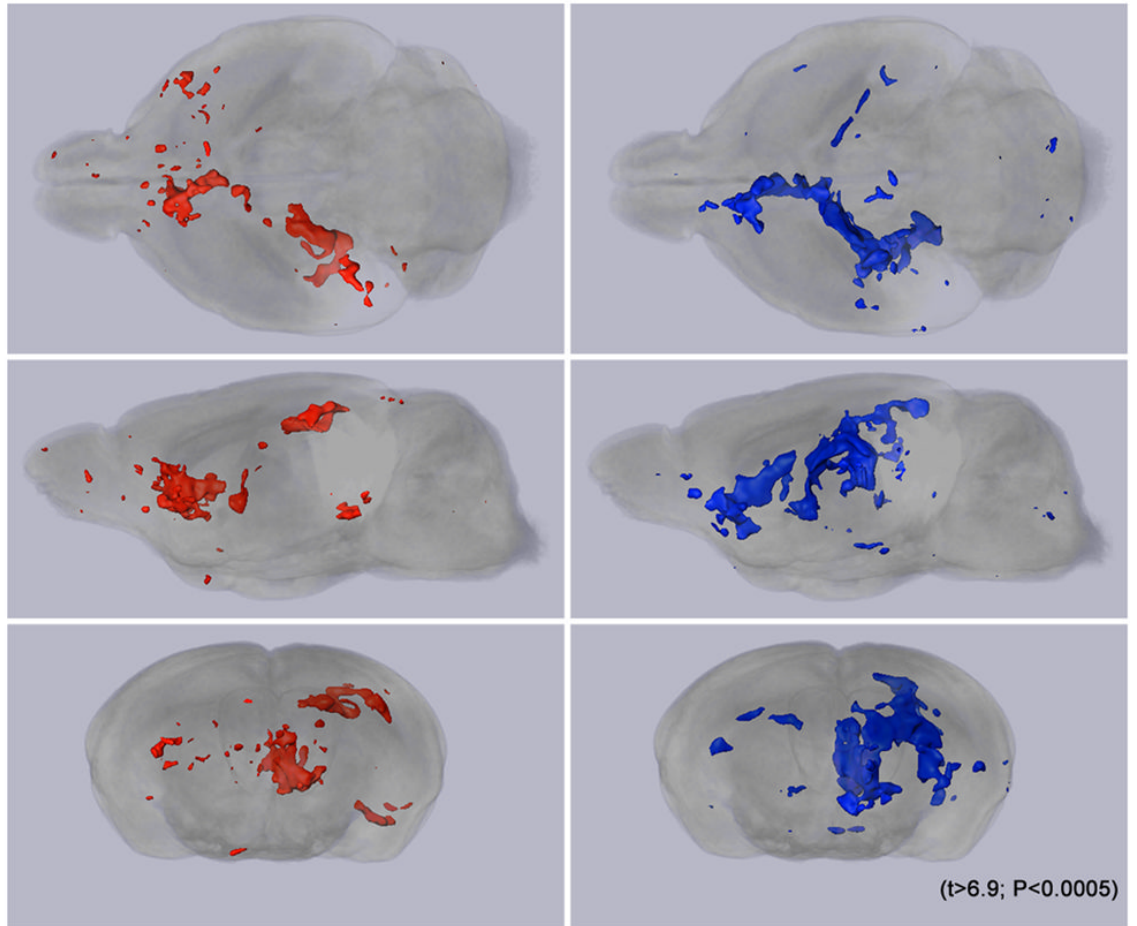


Statistical map: 6 hour > 0.5 hour

2N littermates

Ts65Dn

b



Statistical map: 24 hour > 6 hour

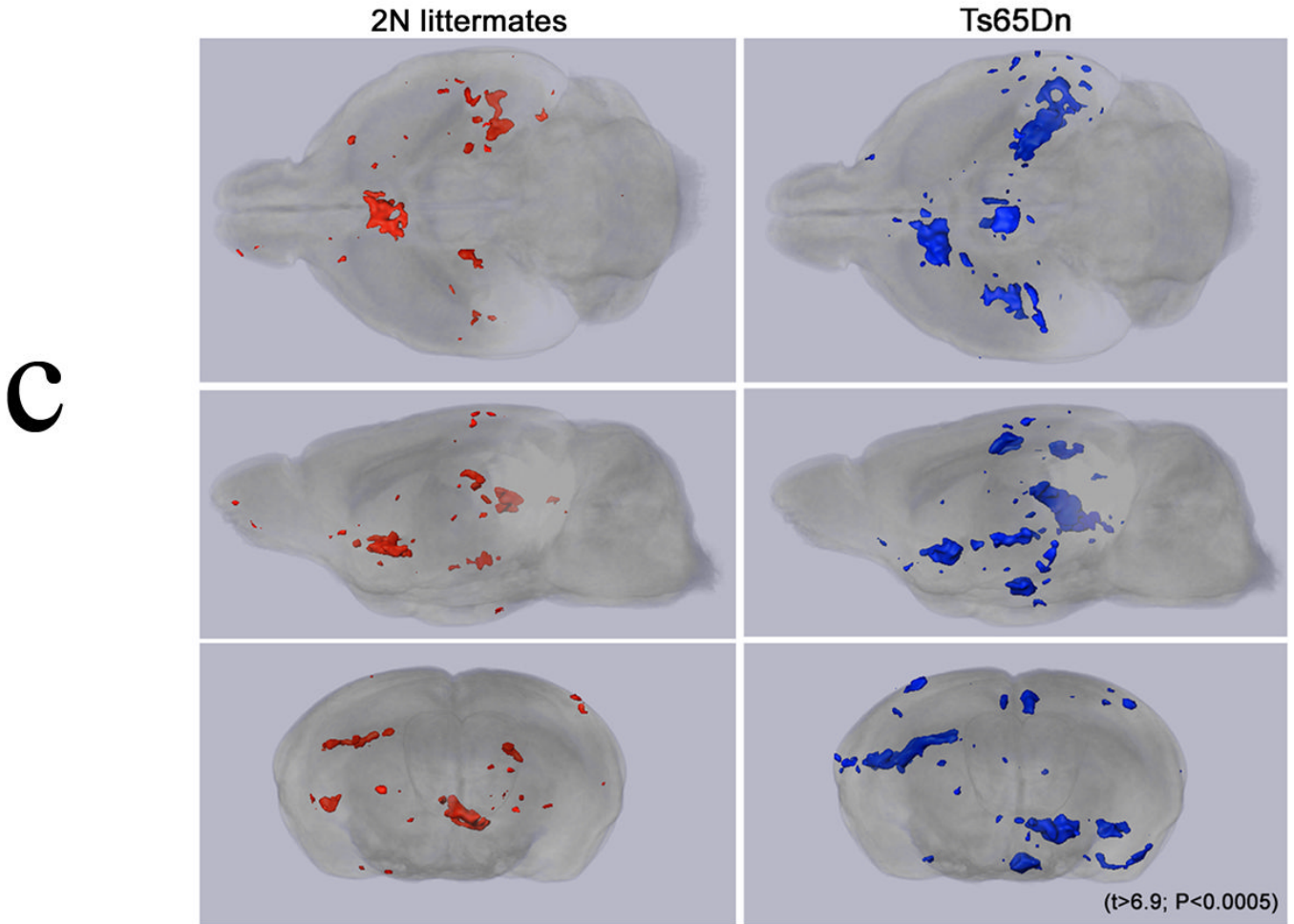


Figure 7. Increased Mn^{2+} transport in the hippocampal-forebrain pathway is apparent in statistical parametric mapping analysis of the MR data

Three views (top, side, end) of the same semitransparent volume projected into two dimensions are shown. Colored voxels (red for 2N and blue for DS) are those places where the intensity is significantly greater at the later time point ($p < 0.0005$). Gray scale background is the 24-hour average image. To appreciate the 3D data, please see Supplemental videos S1–6.

A. SPM of 0.5 hr versus pre-injection data. This map shows the cluster of Mn^{2+} enhanced voxels at the injection site in the hippocampus of both genotypes. Scattered colored voxels outside the injection sites are few and display no particular anatomical pattern. Note the absence of voxels with significantly increased intensity in the hippocampal-septal pathway in this map of 0.5 hr after injection over pre-injection. Also see Supplemental video S1 for 2N littermate, and S2 for Ts65Dn.

B. SPM of 6 hr versus 0.5 hr post-injection data. At 6 hr post Mn^{2+} injection, the expected pathway from hippocampus, along the fimbria, to the septal nuclei in both Ts65DN and 2N littermates contains voxels with significantly increased intensity compared with the 0.5 hr post-injection images. The extent of significantly enhanced voxels is substantially more pronounced in the Ts65Dn. In the basal forebrain voxels with significantly increased intensity occupied 2.4 mm^3 in the Ts65Dn group and only 1.3 mm^3 in the 2N group. In the contralateral hippocampus, voxels with significantly increased intensity occupied 0.4 mm^3 in the Ts65Dn

group and no significantly enhanced voxels were detected there in the 2N group. Also see Supplemental video S3 for 2N littermate, and S4 for Ts65Dn.

C. SPM of 24 hr versus 6 hr post-injection data. Mn^{2+} transport continued along known pathways from 6 to 24 hours with increased intensity in the septal regions and in the hippocampus contralateral to the injection site in both cohorts and into a number of other structures (see Table 1) in the Ts65Dn animals. In the basal forebrain, voxels with significantly increased intensity occupied 1.6 mm³ in the Ts65Dn group and only 0.5 mm³ in the 2N group. In the contralateral hippocampus, voxels with significantly increased intensity occupied 3.1 mm³ in the Ts65DN group 0.2 mm³ in the 2N group and. Also see Supplemental video S5 for 2N littermate, and S6 for Ts65Dn.

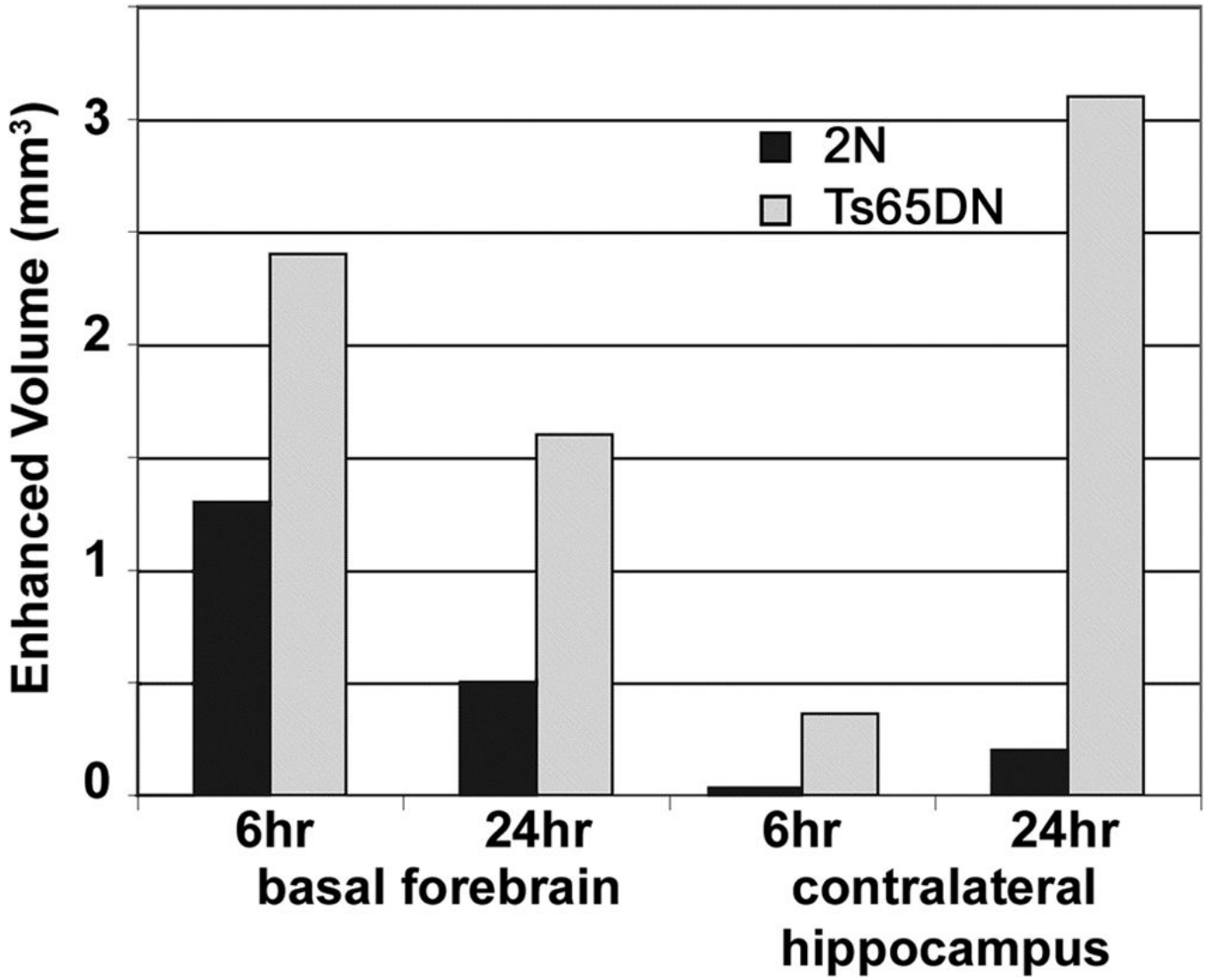


Figure 8. Volume occupied by statistically enhanced voxels is greater in DS than in normal brains
Volumes within basal forebrain and hippocampus contralateral to the injection site occupied by significantly enhanced voxels at 6 hr versus 0.5 hr (6 hr) and 24 hr versus 6 hr (24 hr) post-injection are shown.

Extent of Manganese Transport from Hippocampal Injection SiteMn²⁺ transports along expected pathways more rapidly in DS than in 2N littermates. Structures with statistically significant ($p < 0.0005$) increase in MRI intensity when compared with the previous time point are noted with a “+” sign. Locations are for the ipsilateral side unless otherwise noted. Structures were identified by comparison of MR images with standard mouse brain anatomy (Hof et al., 2000; Paxinos and Franklin, 2001).

Table 1

Location	0.5 hr		6 hr		24 hr	
	2N littermate	Ts65Dn	2N littermate	Ts65Dn	2N littermate	Ts65Dn
Hippocampus CA3	+	+	+	+	+	+
Hippocampus CA1	+	+	+	+	+	+
Molecular layer of the dentate gyrus	+	+	+	+	+	+
Fimbria	-	-	+	+	+	+
Septofimbrial nucleus	-	-	+	+	+	+
Lateral septal nucleus	-	-	+	+	+	+
Medial septal nucleus	-	-	-	+	+	+
Nucleus accumbens core	-	-	-	+	-	+
Anterior olfactory nucleus	-	-	-	+	-	+
Dorsal tectum	-	-	-	+	-	+
Fimbria, contralateral	-	-	-	-	-	+
Hippocampus CA3, contralateral	-	-	-	-	+	+
Bed of nucleus stria terminalis	-	-	-	-	+	+
Ventral pallidum	-	-	-	-	-	+
Ventromedial hypothalamic nuclei	-	-	-	-	-	+
Medial amygdala	-	-	-	-	-	+
Retrosplenial granular cortex	-	-	-	-	-	+